INORGANIC CHEMISTRY FRONTIERS

RESEARCH ARTICLE

View Article Online
View Journal | View Issue

Cite this: *Inorg. Chem. Front.*, 2022, **9**, 2271

The critical role of ligand topology: strikingly different properties of Gd(III) complexes with regioisomeric AAZTA derivatives†

Jonathan Martinelli, [a] Mariangela Boccalon, [b] David Horvath, [b,c] David Esteban-Gomez, [d] Carlos Platas-Iglesias, [d] Zsolt Baranyai [b] and Lorenzo Tei *[a]

The substitution of an acetate pendant arm on the endocyclic or exocyclic nitrogen atoms of AAZTA with a hydroxybenzyl group results in two regioisomeric Gd(III) complexes with different hydration numbers, thermodynamic stabilities differing by 5.5 log *K* units and remarkably different kinetic inertness. The ligand functionalized with the phenol group on the exocyclic N atom (AAZ3A-exoHB) forms a Gd(III) complex with remarkably high stability (log K_{GdL} = 25.06) thanks to the tight coordination of the phenol group, which presents a rather low protonation constant (log K_{GdHL} = 3.22). Conversely, the complex formed with the ligand bearing a phenol unit attached to an endocyclic N atom (AAZ3A-endoHB) is considerably less stable (log K_{GdL} = 19.57) and more prone to protonation (log K_{GdHL} = 6.22). Transmetallation kinetics studies in the presence of Cu(II) evidence that the Gd(III) complexes dissociate *via* the proton- and metal-assisted dissociation pathways, with the AAZ3A-exoHB derivative being considerably more inert. A detailed ^{1}H nuclear magnetic relaxation dispersion (NMRD) study coupled with ^{17}O NMR measurements demonstrates that the complex with AAZ3A-exoHB contains a single water molecule in the inner coordination sphere, while the AAZ3A-endoHB analogue has two water molecules coordinated to the metal ion endowed with significantly different water exchange rates. Finally, a binding study of the two complexes with human serum albumin showed a stronger interaction and higher relaxivity (r_1^b = 36.5 mM^{-1} s^{-1} at 30 MHz and 298 K) for Gd(AAZ3A-endoHB) than for Gd(AAZ3A-exoHB). Overall, this study highlights the importance that ligand topology has in the properties of Gd(III) complexes relevant in the field of magnetic resonance imaging (MRI).

Received 28th February 2022,
Accepted 28th March 2022

DOI: 10.1039/d2qi00451h

rsc.li/frontiers-inorganic

Introduction

Among the macrocyclic or mesocyclic polydentate ligands used for imaging applications, AAZTA (6-amino-6-methylperhydro-1,4-diazepine tetraacetic acid, Scheme 1) is one of the most versatile platforms with remarkable affinity for both di- and trivalent metal ions.[1–6] The first and most investigated use of this heptadentate chelator is the preparation of the bis-hydrated Gd(III) complex, which displays excellent properties for its application as a magnetic resonance imaging (MRI) contrast agent (CA).[1] Furthermore, the same ligand has been used to complex efficiently radiometals such as ^{68}Ga[2,3] and ^{44}Sc[4,5] for Positron Emission Tomography (PET) and other lanthanide ions like Yb(III) or Tm(III) for chemical exchange saturation transfer (CEST) studies.[7,8] It has also been recently reported that, passing from Gd(III) to Yb(III), Ln(AAZTA) complexes change the number of coordinated water molecules from two (q = 2) to one (q = 1) as their

[a]*Dipartimento di Scienze e Innovazione Tecnologica, Università del Piemonte Orientale "A. Avogadro", Viale T. Michel 11, 15121 Alessandria, Italy. E-mail: lorenzo.tei@uniupo.it*
[b]*Bracco Research Centre, Bracco Imaging S.p.A., Via Ribes 5, 10010 Colleretto Giacosa, Italy*
[c]*University of Debrecen, Faculty of Science and Technology, Department of Physical Chemistry, Doctoral School of Chemistry, Debrecen, Hungary*
[d]*Universidade da Coruña, Centro de Investigacións Científicas Avanzadas (CICA) and Departamento de Química Fundamental, Facultade de Ciencias, 15071 A Coruña, Galicia, Spain*

†Electronic supplementary information (ESI) available: Characterizations of the ligands; supplementary figures and tables. See DOI: https://doi.org/10.1039/d2qi00451h

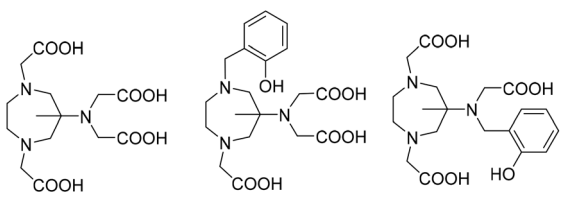

AAZTA AAZ3A-endoHB AAZ3A-exoHB

Scheme 1 Structures of the ligands discussed or mentioned in this work.

exchange rate decreases by several orders of magnitude.[8] Moreover, X-ray structural studies and DFT calculations have shown that the complexes adopt a monocapped square antiprismatic structure when q = 2 and a dodecahedral structure when q = 1.[7,8] Finally, it has been recently highlighted by ^{1}H relaxometric, ^{17}O NMR and DFT studies that $[Gd(AAZTA)(H_2O)_2]^-$ presents one Gd-bound water molecule with an exchange rate 6 times faster than the other, due to a longer metal–water distance.[9]

Notably, another heptadentate ligand that forms a very inert Gd(III) complex is the functionalized tris-serinolamido PCTA derivative (Gadopiclenol) that shows remarkable relaxivity values due to its large molecular weight and the presence of hydrophilic polyalcohol pendants that favour the additional contribution of second sphere water molecules.[10]

The modification of the ligand AAZTA has been pursued with the intent to form more rigid ligands to increase the kinetic inertness of the resulting Gd(III) or Ga(III) complexes[11,12] and bifunctional chelates suitable for building multimeric structures,[13] for conjugation to targeting vectors,[2–5] nanoparticles or hydrophobic moieties.[14,15] However, the modification of the coordination cage with different pendant arms received limited attention.[16,17] Only a derivative in which the two acetate groups on the diazepine ring were replaced by methylphosphinate pendant arms[16] and mono- and bis-phosphonate derivatives[17] have been reported. In these examples, however, the presence of a more hindering phosphonate or phosphinate group reduces the space available for the coordination of one water molecule, thus reducing the relaxivity of the final Gd(III) complex. Moreover, two diastereoisomeric di-glutarate AAZTA derivatives were reported forming Gd(III) complexes with different water exchange rates, in both cases lower than that of GdAAZTA.[59]

The importance of the donor group in the coordination of the metal ion and in the properties of the resulting metal complexes requires special attention in the choice of the functional group. Phenolate anions are more basic than carboxylates and thus can be strong donor groups for hard metal ions, although they are easier to protonate in acidic media. In fact, macrocyclic and acyclic chelates functionalized with hydroxybenzyl units are mainly reported in the literature as ligands for hard metal ions such as Fe(III) and Ga(III).[18]

In this study, we replaced one acetate pendant arm from the AAZTA structure with hydroxybenzyl moieties and synthesized two regioisomeric ligands shown in Scheme 1 (namely AAZ3A-endoHB and AAZ3A-exoHB) with the aim to study the influence of the phenolate donor on the solution properties of the resulting Gd(III) complexes. The different topologies of the two ligands result in Gd(III) complexes astonishingly diverse in terms of thermodynamic stability and kinetic inertness, key properties for the design of chelates for biomedical application.

Results and discussion

Synthesis of the ligands

The synthesis of the two ligands started from an appropriately substituted 6-aminodiazepine[19] (**1** and **3** in Scheme 2) and proceeded *via* a series of alkylations, hydrogenation and deprotection steps. In particular, AAZ3A-endoHB was obtained by removal of the benzyl group of **1** through catalytic hydrogenation, introduction of the protected hydroxybenzyl moiety *via* substitution with 2-(bromomethyl)phenyl acetate (BMPA) and final deprotection of the functional groups through basic hydrolysis followed by acidic treatment. On the other hand, AAZ3A-exoHB was synthesized by alkylation of the secondary amine of **3** with *tert*-butyl bromoacetate followed by deprotection of the *tert*-butyl ester moieties.

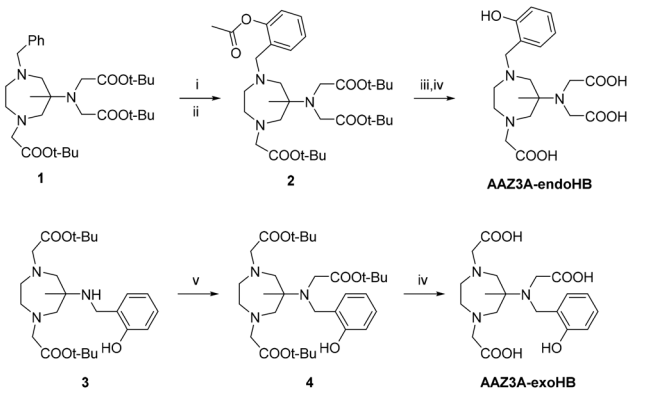

Scheme 2 Synthesis of ligands AAZ3A-endoHB and AAZ3A-exoHB: (i) H_2, 10% Pd/C, rt, overnight; (ii) BMPA, K_2CO_3, MeCN, reflux, overnight; (iii) 1 M NaOH, 1 : 1 H_2O/THF, 60 °C, 3 h; (iv) 1 : 1 DCM/TFA, rt, overnight; (v) $BrCH_2COOtBu$, K_2CO_3, MeCN, reflux, overnight.

Thermodynamic properties

Considering the key importance of the thermodynamic properties of any metal-complex proposed for *in vivo* applications, the equilibrium properties of the two regioisomeric ligands and those of the Gd(III) complexes were investigated in detail. First of all, the protonation constants of both ligands, defined by eqn (1), were determined by pH-potentiometry and the $\log K_i^H$ values are listed in Table 1.

$$K_i^H = \frac{[H_iL]}{[H_{i-1}L][H^+]} \quad (1)$$

Comparing the $\log K_i^H$ values of the two ligands with those of AAZTA, it is clear that the main difference is observed for $\log K_2^H$, which can be ascribed to the phenolate group. To confirm this, the protonation sequence of AAZ3A-endoHB was also determined by recording the absorption spectra of the ligand in the pH range 2.0–11.5 (Fig. S1†). According to the spectral changes, it can be assumed that the $\log K_i^H$ = 9.2 (1) value characterizes the protonation of the phenolate group of the AAZ3A-endoHB ligand, as it is also very similar to the pK_a of phenol ($\log K^H$ = 10.0, 0.1 M $NaClO_4$, 25 °C).[20]

A comparison of the protonation constants (Table 1) indicates that the $\log K_1^H$ value of AAZ3A-exoHB is slightly higher than that of AAZ3A-endoHB, which can be explained by the H-bonding between the phenolate group and the protonated exocyclic N-atom which is less likely to occur in case of AAZ3A-

Table 1 Protonation constants ($\log K_i^H$) of AAZ3A-endoHB and AAZ3A-exoHB compared with AAZTA and an AAZTA-like ligand (CyAAZTA); stability ($\log K_{GdL}$) and protonation constants ($\log K_{Gd(HiL)}$) of Gd(AAZ3A-endoHB), Gd(AAZ3A-exoHB), Gd(CyAAZTA) and Gd(AAZTA) complexes (25 °C). Standard deviations are shown in parentheses

	AAZ3A-exoHB	AAZ3A-endoHB	CyAAZTA[11,12]	AAZTA	
I	0.15 M NaCl		0.1 M KCl	0.15 M NaCl[21,22]	0.1 M KCl[23]
$\log K_1^H$	12.14 (1)	11.47 (4)	10.48	10.06	11.23
$\log K_2^H$	10.66 (2)	9.18 (2)	6.43	6.50	6.52
$\log K_3^H$	5.82 (4)	6.17 (3)	4.23	3.77	3.78
$\log K_4^H$	3.84 (4)	3.76 (3)	2.76	2.33	2.24
$\log K_5^H$	2.88 (4)	2.69 (3)	1.68	1.51	1.56
$\log K_6^H$	1.34 (3)	1.43 (2)	—	—	—
$\Sigma\log K_i^H$	36.69	32.14	25.58	24.16	25.33
$\log K_{GdL}$	25.06 (4)	19.57 (5)	18.26	18.93	20.24
$\log K_{GdHL}$[a]	3.22 (3)	6.22 (3)	3.79	2.18	1.89
$\log K_{GdH_2L}$	2.51 (6)	3.44 (4)	—	—	—
$\log K_{GdLH-1}$	—	10.51 (4)	—	—	—
pGd[b]	**18.00**	**14.67**	**16.10**	**17.17**	**17.31**

[a] Protonation constants of the phenol group obtained by spectrophotometry: Gd(AAZ3A-endoHB), $\log K_{GdHL}$ = 5.82 (2); Gd(AAZ3A-exoHB, $\log K_{GdHL}$ = 3.99 (4), 0.15 M NaCl, 25 °C. [b] $pG_d = -\log[Gd(III)]_{free}$, $[Gd(III)]_{tot}$ = 1 μM, $[L]_{tot}$ = 10 μM, pH = 7.4.[24]

endoHB. On the other hand, $\log K_1^H$ of AAZTA (in 0.15 M NaCl) is significantly lower due to the formation of a Na^+ complex competing with the first protonation process.[21,22] The lower affinity of AAZ3A-endoHB and AAZ3A-exoHB towards Na^+ maybe related to the formation of a H-bond between the protonated nitrogen and the basic phenolate group, which can hinder the interaction of the ligands with the Na^+ ion.

The stability and protonation constants of the Gd(III)-complexes, calculated from the titration curves obtained at 1 : 1 metal to ligand concentration ratios, are reported in Table 1 and defined by eqn (2)–(4):

$$K_{GdL} = \frac{[GdL]}{[Gd^{3+}][L]} \quad (2)$$

$$K_{GdH_iL} = \frac{[Gd(H_iL)]}{[Gd(H_{i-1}L)][H^+]} \quad (3)$$

$$K_{GdLH_{-1}} = \frac{[GdL]}{[Gd(L)OH^-][H^+]} \quad (4)$$

where i = 1–3. The best fitting was obtained by using a model that includes the formation of GdL, GdHL and GdH_2L species in equilibrium. The titration data of AAZ3A-endoHB in the presence of Gd(III) indicate base consuming processes at pH > 9. These processes can be interpreted by assuming the hydrolysis of the metal ion; the coordination of an OH^- ion results in the formation of Gd(L)OH species characterized by the equilibrium constant K_{GdLH-1} (eqn (4)).

The deprotonation of the phenol group in the Gd(III) complexes was studied by spectrophotometry following the absorbance values at 238, 275 and 291 nm of the aromatic group of the ligand (Fig. S2 and S3†). The protonation constants of the phenol group in the Gd(III) complexes were calculated by fitting the absorbance–pH data pairs to eqn (S3).†

While the stability constant of Gd(AAZ3A-endoHB) is comparable with those of AAZTA and CyAAZTA complexes, the data in Table 1 evidence a $\Delta\log K_{GdL}$ between the two regioisomers of 5.49 units in favour of Gd(AAZ3A-exoHB), due to the stronger interaction between the Gd(III) ion and the basic exocyclic phenolate-O^- donor than with the endocyclic phenolate. This stronger interaction can be further highlighted by the $\log K_{GdHL}$ values related to the protonation of the phenolate donor atom, which is about 3 $\log K$ unit smaller in Gd(AAZ3A-exoHB) than for Gd(AAZ3A-endoHB). Interestingly, the stability constants of Gd(AAZ3A-exoHB) and Gd(DOTA) are comparable and significantly higher (*ca.* 3 $\log K$ units) than that of Gd(DTPA) measured in the same experimental conditions (Gd(DOTA): $\log K_{GdL}$ = 24.7; Gd(DTPA): $\log K_{GdL}$ = 22.03).[25,26] To the best of our knowledge Gd(AAZ3A-exoHB) is characterized by the highest thermodynamic stability among the Gd(III) complexes formed with heptadentate ligands.

Furthermore, a second lower protonation constant could be determined by pH-potentiometric studies for both Gd(III) complexes, probably due to one more weakly coordinated donor atom (a carboxylate-O), which can be protonated in the pH range 2–5. By taking into account the equilibrium data in Table 1, the species distribution diagrams of the Gd(III)–AAZ3A-endoHB and Gd(III)–AAZ3A-exoHB systems were calculated as a function of pH and shown in Fig. S4 and S5.†

Kinetic inertness

The kinetic inertness of Gd(AAZ3A-endoHB) and Gd(AAZ3A-exoHB) was determined by following the transmetallation reactions between the Gd(III) complexes and the Cu(II) ion *via* spectrophotometry. These experiments were monitored on the absorption band of the resulting Cu(II) complexes in the pH range 2.8–5.0 in the presence of a Cu(II) excess to guarantee the pseudo-first order kinetic condition ([GdL] = 0.2 mM, [Cu(II)] = 2.0–8.0 mM, 0.15 M NaCl, 25 °C). The proposed mechanism for the transmetallation of Gd(III)-complexes is shown in Scheme 3, whereas the definitions and equations used for the evaluation of the kinetic data are reported in the ESI.†

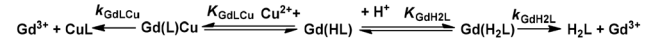

Scheme 3 Proton- and metal-assisted dissociation of Gd(AAZ3A-endoHB) and Gd(AAZ3A-exoHB) complexes.

The kinetic data (Fig. S8 and S9†) show that the k_d values increase with increasing $[H^+]$ (particularly at lower [Cu(II)]) and decrease with increasing [Cu(II)] at pH < 4.0. By taking into account the species distribution of the Gd(III)–L systems, the increase in the k_d values with increasing $[H^+]$ can be interpreted in terms of the formation (K_{GdH_2L}, eqn (3)) and the slow dissociation of protonated $Gd(H_2L)$ intermediate (k_{GdH_2L}, eqn (S6)†), which is followed by a fast reaction between the free ligands and the exchanging Cu(II) metal ions. The transmetallation reaction can also occur *via* direct attack of the exchanging metal ion on the Gd(III) complex (k_{GdLCu}, eqn (S8)†), through the formation of a dinuclear intermediate (K_{GdLCu}, eqn (S7)†). The formation of the dinuclear [Lu(AAZTA)]Cu complex was also observed by ^{1}H NMR spectroscopy in the presence of a large excess of the Cu(II) ion.[23] It can be assumed that in the dinuclear intermediate Gd(L)Cu, the functional groups of the ligand are slowly transferred from Gd(III) to the attacking Cu(II) step by step (eqn (S7)†). The $k_1 = k_{GdH_2L} \times K_{GdH_2L}$ and $k_3 = k_{GdLCu} \times K_{GdLCu}$ rate constants, as well as the protonation and stability constants K_{GdH_2L} and K_{GdLCu} characterizing the proton- and metal-assisted dissociation for the two complexes, are shown in Table 2 and compared with the corresponding values of Gd(AAZTA) and Gd(CyAAZTA).

The k_1 rate constant characterizing the proton-assisted dissociation of Gd(AAZ3A-exoHB) is about 60 times smaller than that of Gd(AAZ3A-endoHB). Based on the mechanism of the proton-assisted dissociation, the protonated intermediates facilitate the proton transfer from the carboxylic acid/phenol groups to the N-atom of the ligand backbone *via* the formation of a relatively labile protonated intermediate. The proton of this intermediate can displace the Gd(III) ion from the coordination cage resulting in the dissociation of the GdL complex. The stronger interaction between the Gd(III) ion and the phenol group in Gd(AAZ3A-exoHB) results in a less probable proton transfer and slower rate of de-coordination of the Gd(III) ion from the N-donor atoms. Moreover, the transfer of the phenol-OH proton to the endocyclic N atom is more likely for $Gd(H_2$AAZ3A-endoHB) than for $Gd(H_2$AAZ3A-exoHB), which can cause the faster H^+-assisted dissociation of the former Gd(III) complex. However, the proton-assisted dissociation of both Gd(III) complexes is faster than for Gd(AAZTA) and Gd(CyAAZTA), which might be interpreted by the electrostatic repulsion between the protonated phenol-OH group and the metal centre of $Gd(H_2L)$ intermediates, which might weaken the interaction between the ring N donor atoms and the Gd(III) ion in Gd(AAZ3A-endoHB) and Gd(AAZ3A-exoHB) complexes. The k_3 rate constants characterizing the Cu(II) assisted dissociation of Gd(AAZ3A-exoHB) is 75 times slower than that of Gd(AAZ3A-endoHB). These findings suggest that the coordination cage around the Gd(III) ion in the Gd(AAZ3A-exoHB) complex is more compact, hindering the transformation of the dinuclear intermediate to the final Cu(II) complex. The stability constants of the dinuclear intermediates formed by Gd(AAZ3A-exoHB) and Gd(AAZ3A-endoHB) with Cu(II) are very similar and somewhat higher than that of Gd(AAZTA), as a consequence of the more basic phenolate pendant group. Finally, the 60 times slower dissociation rate constant (k_d) and higher half-lives ($t_{1/2} = \ln 2/k_d$, pH = 7.4, 25 °C) for Gd(AAZ3A-exoHB) indicate that this complex is remarkably more inert than Gd(AAZ3A-endoHB).

Structural properties

The relaxivity values (r_1) for Gd(AAZ3A-endoHB) and Gd(AAZ3A-exoHB) at 30 MHz, 25 °C and pH 7.0 (Table 3) are 7.3 and 5.4 mM^{-1} s^{-1}, respectively, and reflect different hydration states for the two complexes, consistent with the presence of two water molecules in the inner coordination sphere of the metal ion for Gd(AAZ3A-endoHB) (q = 2) and one for Gd(AAZ3A-exoHB) (q = 1).

Density Functional Theory (DFT) calculations were performed to rationalise the strikingly different behaviour of the regioisomeric Gd(III) complexes. We performed calculations on the $[Gd(L)(H_2O)_2]^-\cdot 4H_2O$ systems (L = AAZ3A-endoHB or AAZ3A-exoHB) at the wB97XD/LCRECP/6-311G(d,p) level,[27,28] including an explicit second-sphere solvation shell[29] and a polarized continuum to model bulk solvent effects (see Computational details below). Calculations performed for the

Table 2 Rate (k_i) and equilibrium (K_i) constant characterizing the transmetallation reaction of Gd(III) complexes formed with AAZTA derivatives (25 °C)

I	Gd(AAZ3A-exoHB) 0.15 M NaCl	Gd(AAZ3A-endoHB)	Gd(CyAAZTA)[12] 0.1 M KCl	Gd(AAZTA)[23] 1.0 M KCl
k_1 (M^{-1} s^{-1})	5.1 ± 0.2	300 ± 30	6.0×10^{-3}	1.05
k_2 (M^{-2} s^{-1})	—	—	53	—
k_3^{Cu} (M^{-1} s^{-1})	$(4 \pm 1)\times 10^{-3}$	0.30 ± 0.05	—	1.9×10^{-4}
K_{GdH_2L} (M^{-1})	238 ± 37	2400 ± 600	6166 (GdHL)	233 (GdHL)
K_{GdLCu} (M^{-1})	27 ± 7	37 ± 10	—	9
k_d (s^{-1}) pH = 5.0	5.1×10^{-5}	2.9×10^{-3}	6.2×10^{-8}	1.0×10^{-5}
$t_{1/2}$ (h) pH = 5.0	3.76	0.07	3106	18.4
k_d (s^{-1}) pH = 7.4	2.0×10^{-7}	1.1×10^{-5}	2.4×10^{-10}	4.0×10^{-8}
$t_{1/2}$ (h) pH = 7.4	939	15.8	8.0×10^{5}	4.3×10^{3}

$[Gd(AAZ3A\text{-}endoHB)(H_2O)_2]^-\cdot 4H_2O$ system predicted a nine-coordinated structure with two inner-sphere water molecules (Fig. 1), which is more stable than the octacoordinated species by $\Delta G^\circ = 6.6$ kJ mol^{-1}. The reverse situation is observed for the $[Gd(AAZ3A\text{-}exoHB)(H_2O)_2]^-\cdot 4H_2O$ complex, the octacoordinated species being favoured by $\Delta G^\circ = 12.9$ kJ mol^{-1}. This is in nice agreement with the experimental ^{17}O NMR data (see below). The analysis of the thermodynamic contributions shows that the hydration reactions $[Gd(L)(H_2O)_2]^- \rightleftarrows [Gd(L)(H_2O)]^- + H_2O$ are characterised by similar negative reaction entropies with the enthalpy contribution being the main responsible for the different hydration numbers (Tables S1–S4, ESI†).

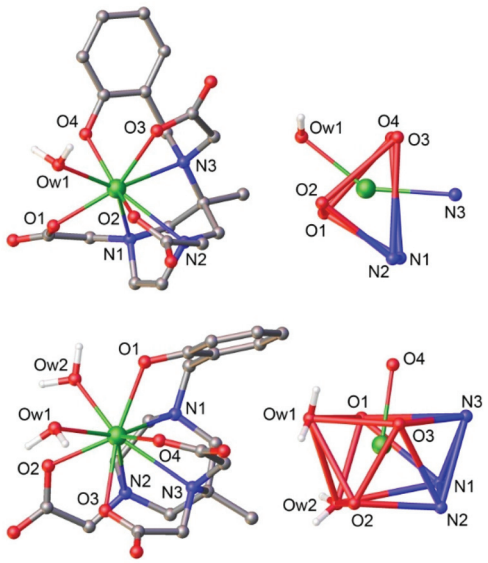

Fig. 1 Structures of the $[Gd(AAZ3A\text{-}endoHB)(H_2O)_2]^-$ (bottom) and $[Gd(AAZ3A\text{-}exoHB)(H_2O)]^-$ (top) systems obtained with DFT calculations. Second-sphere water molecules are omitted for simplicity. Bond distances (Å), $[Gd(AAZ3A\text{-}endoHB)(H_2O)_2]^-$: Gd–N1, 2.734; Gd–N2, 2.725; Gd–N3, 2.701; Gd–O1, 2.391; Gd–O2, 2.426; Gd–O3, 2.402; Gd–O4, 2.452; Gd–O1w, 2.515; Gd–O2w, 2.518. $[Gd(AAZ3A\text{-}exoHB)(H_2O)]^-$: Gd–N1, 2.661; Gd–N2, 2.649; Gd–N3, 2.681; Gd–O1, 2.403; Gd–O2, 2.421; Gd–O3, 2.360; Gd–O4, 2.325; Gd–O1w, 2.470.

The coordination polyhedron around the Gd(III) ions in $[Gd(AAZ3A\text{-}endoHB)(H_2O)_2]^-$ can be described as a capped square antiprism, where the capping position is occupied by an oxygen atom of one of the carboxylate groups. Conversely, the coordination polyhedron in $[Gd(AAZ3A\text{-}exoHB)(H_2O)]^-$ is a biaugmented trigonal prism, with the exocyclic N atom and the coordinated water molecule occupying the capping positions (Fig. 1). The most important difference in bond distances is observed for the Gd(III)–O_{phenol} bond, which is considerably shorter for $[Gd(AAZ3A\text{-}exoHB)(H_2O)]^-$ (Gd–O4 = 2.325 Å) than for $[Gd(AAZ3A\text{-}endoHB)(H_2O)_2]^-$ (Gd–O1 = 2.391 Å). This indicates that the phenolate group in the latter complex occupies a sterically demanding position, resulting in a weaker interaction with the metal ion. As a result, the phenolate group in the $[Gd(AAZ3A\text{-}endoHB)(H_2O)_2]^-$ complex is characterised by a higher protonation constant ($\log K_{GdHL} = 6.22$) than the $[Gd(AAZ3A\text{-}exoHB)(H_2O)]^-$ regioisomer ($\log K_{GdHL} = 3.22$). Thus, the presence of the bulky phenolate group attached to the endocyclic N atom introduces an important steric hindrance for the coordination to the Gd(III) ion, an effect that is clearly reflected in the impressive difference in stability of the two complexes. A weak coordination of the phenolate group in $[Gd(AAZ3A\text{-}endoHB)(H_2O)_2]^-$ likely facilitates the protonation of the complex, and thus its dissociation following the acid-catalysed mechanism.

Relaxation properties

The relaxometric characterization of the Gd(III) complexes started by measuring the pH dependence of r_1 for the two Gd^{III} complexes to assess possible variations of hydration state or coordination environment with pH (Fig. S13 and S14†). In particular, r_1 of Gd(AAZ3A-endoHB) is almost constant from pH = 3 to pH = 11. This indicates that over this broad range of pH values the complex does not hydrolyze and does not vary the hydration number q. In case of Gd(AAZ3A-exoHB), a slight and constant decrease of r_1 from pH 4 to pH 7 is observed

Table 3 Parameters obtained from the fits of ^{17}O NMR and ^{1}H NMRD data for Gd(AAZ3A-endoHB) and Gd(AAZ3A-exoHB)[a,b]

Parameter	Gd(AAZ3A-endoHB)	Gd(AAZ3A-exoHB)	Gd(AAZTA)[1,8]
$^{298}r_1$ (30 MHz, pH 7) (mM^{-1} s^{-1})	7.3 ± 0.1	5.4 ± 0.1	7.1
$\Delta^2/10^{19}$ s^{-2}	8.6 ± 0.3	2.0 ± 0.2	2.2
$^{298}\tau_V$/ps	16.2 ± 1.1	29.1 ± 1.6	31
$^{298}\tau_M^A$/ns	35 ± 3	20 ± 1	29
ΔH_M^A/kJ mol^{-1}	15.0 ± 0.5	15.9 ± 0.4	20
$^{298}\tau_M^B$/ns	290 ± 10	—	169
ΔH_M^B/kJ mol^{-1}	20.0 ± 0.3	—	29.5
$A_O^A/\hbar/10^6$ rad s^{-1}	−3.3 ± 0.1	−3.3 ± 0.1	−3.8
$A_O^B/\hbar/10^6$ rad s^{-1}	−3.6 ± 0.1	—	−3.9
$298\tau_R$/ps	79 ± 2	80 ± 1	74
q	2	1	2

[a] Some of the parameters affecting r_1 and the ^{17}O NMR data were fixed to the values reported in literature for GdAAZTA; the water proton-gadolinium distance (r = 3.05 Å), the outer sphere relaxation parameters (a = 4.0 Å, $^{298}D = 2.24 \times 10^5$ cm^2 s^{-1}) and the activation energy for the diffusion coefficient (E_D = 20 kJ mol^{-1}). Then, the activation energies of τ_V (E_V) and τ_R (E_R) were set to 1.0 and 18.0 kJ mol^{-1}, respectively, and the distance r_{GdO} was fixed at 2.5 Å. [b] Information on q and on the scalar coupling $A_O/\hbar$ are derived from the temperature dependence of $\Delta\omega_r$.

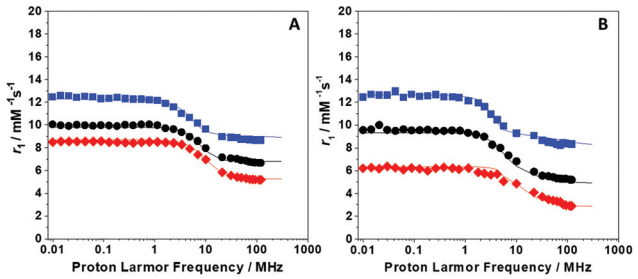

Fig. 2 ^{1}H nuclear magnetic relaxation dispersion (NMRD) profiles at pH 7.0 of Gd(AAZ3A-endoHB) (A) and Gd(AAZ3A-exoHB) (B) recorded at different temperatures 283 K (■), 298 K (●) and 310 K (◆). The solid lines correspond to the fits of the data as described in the text.

(from about 7 to 5.5 mM^{-1} s^{-1}) and then it remains almost constant going to basic pH. The slightly higher r_1 at acidic pH maybe due to several reasons: (1) the presence of an equilibrium between q = 1 and q = 2 species occurring after protonation of the phenolate oxygen as can be seen from the species distribution diagram in Fig. S5;† (2) a contribution to the relaxivity of acid catalyzed proton exchange or (3) second sphere water molecules. Finally, for both complexes, at pH < 3 r_1 increases likely because of proton-assisted metal release.

Then, the ^{1}H nuclear magnetic relaxation dispersion (NMRD) profiles (Fig. 2) and the temperature dependence of the transverse ^{17}O NMR relaxation rate (R_{2r}) and chemical shifts ($\Delta\omega_r$) were recorded for both complexes (Fig. 3 and S10, S11†). Notably, the shape of the variable-temperature ^{17}O NMR R_2 profile of Gd(AAZ3A-endoHB) (Fig. 3A) evidences the presence of two water molecules with significantly different water exchange dynamics; in fact, the curve is distant from the simple pseudo-exponential decay expected for systems containing one (or two) coordinated water molecule(s) in exchange with bulk solvent, as shown, conversely, by the ^{17}O R_2 profile of Gd(AAZ3A-exoHB) (Fig. 3B). ^{1}H NMR spectra recorded for the Eu(AAZ3A-endoHB) complex (273–313 K, Fig. S15†) exclude that the shape of the ^{17}O NMR R_2 profile is related to the presence of different coordination isomers with water molecules exchanging at different rates, as observed in the case of some GdDOTA-like complexes.[30] Another possibility considers the

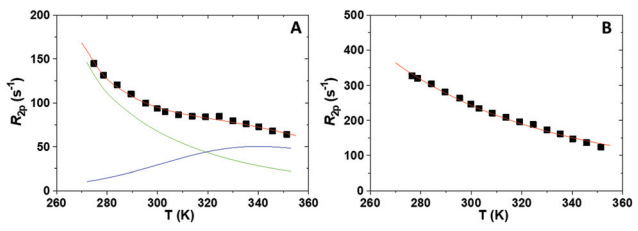

Fig. 3 ^{17}O NMR transverse relaxation rates as a function of temperature measured at pH 7.0 and 500 MHz (11.74 T) for Gd(AAZ3A-endoHB) (A, 2.6 mM) and Gd(AAZ3A-exoHB) (B, 12.3 mM). The solid lines correspond to the fits of the data as described in the text, while the blue and green lines in (A) represent the calculated contributions of the two different water species, in faster and slower exchange with the bulk, respectively.

presence of a mixture of a protonated and a non-protonated species at about 1 : 1 ratio at pH 7 with substantially different water exchange rates. Thus, ^{17}O NMR data were recorded also at pH 5 and 8 for Gd(AAZ3A-endoHB) (Fig. S12†) where the species with the protonated and deprotonated phenol, respectively, are predominating (see Fig. S10†). The qualitative analysis of the profiles highlights that at acidic pH both water molecules exchange faster, whereas at pH 8 there is no difference with the profile at pH 7. Therefore, we can exclude that the two species exchanging differently are the protonated and deprotonated complexes.

Thus, the ^{17}O NMR and NMRD data for Gd(AAZ3A-endoHB) were analysed by considering the presence in solution of two water molecules subject to different exchange rates, whereas for Gd(AAZ3A-exoHB) the analysis considered the presence of a q = 1 complex. The ^{1}H NMRD and ^{17}O NMR data (Fig. 2 and 3), were fitted simultaneously according to the established theory of paramagnetic relaxation.[31] The data for Gd(AAZ3A-endoHB) were well reproduced by considering that the two Gd(III)-bound water molecules are characterized by significantly different residence lifetimes (τ_M^A = 35 ns and τ_M^B = 290 ns) and enthalpies associated to the exchange process (ΔH_M^A = 15 kJ mol^{-1} and ΔH_M^B = 20 kJ mol^{-1}). The water molecule residing for shorter times on the metal center (A) exchanges more than 8 times faster than the other with a reaction enthalpy 1.3 times lower.

As observed for Gd(AAZTA),[8] it is reasonable to assume that breaking the Gd–O bond of the water molecule less strongly bound to the metal centre and with a longer Gd–O distance requires the lowest energy. In case of Gd(AAZ3A-exoHB) the coordinated water molecule exchanges very fast with the bulk ($^{298}\tau_M$ = 20 ns), similar to the faster water molecule of Gd(AAZ3A-endoHB) and more than four times faster than that measured for other GdAAZTA-like complexes.[1,12] The higher water exchange rate may be ascribed to the increased steric compression near the water coordination site imposed by the phenolate donor group, as shown already in cases where a six-membered chelate ring is formed.[32,33]

Moreover, τ_R values around 80 ps and the electronic parameters characterizing the two complexes are in line with the corresponding values obtained for GdAAZTA-like complexes.[1,12] The fitted ^{17}O hyperfine coupling constants for Gd(AAZ3A-endoHB) show a higher value for the more strongly bound and more slowly exchanging water molecule ($A_O/\hbar^A$ = −3.3 × 10^6 rad s^{-1}, $A_O/\hbar^B$ = −3.6 × 10^6 rad s^{-1}) whereas for Gd(AAZ3A-exoHB) the value is similar to that of the faster exchanging molecule (−3.3 × 10^6 rad s^{-1}).

Relativistic DFT calculations (TPSSh/SARC2-DKH-QZVP/DKH-def2-TZVPP[34–37] see below) provide calculated values in excellent agreement with the experiment ($A_O/\hbar^A$ = −3.0 × 10^6 rad s^{-1} and $A_O/\hbar^B$ = −3.6 × 10^6 rad s^{-1} for Gd(AAZ3A-endoHB), $A_O/\hbar^B$ = −3.7 × 10^6 rad s^{-1} for Gd(AAZ3A-exoHB), confirming that the hydration numbers assumed for the analysis of the ^{1}H NMRD and ^{17}O NMR data are correct. The zero field splitting (ZFS) parameters obtained using NEVPT2 calculations (Table S5, ESI†) provide Δ^2 values of 8.1 × 10^{19} and 6.5 × 10^{19} rad^2 s^{-2} for [Gd(AAZ3A-endoHB)(H$_2$O)$_2$]$^-$ and [Gd(AAZ3A-

exoHB)$(H_2O)]^-$, respectively, again in reasonable agreement with the experiment. The lower value of Δ^2 calculated for the latter complex appears to be related to the smaller splitting of the four Kramer doublets associated to the $^8S_{7/2}$ ground state.

Interaction with human serum albumin (HSA)

We argued that the presence of a phenol ring in these Gd(III)-complexes would enable non-covalent interaction with hydrophobic binding sites on HSA, the most abundant serum protein in blood and a primary biological target for MRI contrast agents. In fact, the formation of supramolecular adducts between a paramagnetic probe and HSA is accompanied by a strong enhancement of the relaxivity because of the decreased tumbling rate of the system. This is generally exploited for increasing the lifetime of the probe in the vascular system for angiographic MRI applications. Notably, in the case of Gd(AAZ3A-endoHB) and Gd(AAZ3A-exoHB) the phenolate group can act both as donor group for the lanthanide ion and as hydrophobic group for HSA interaction. The longitudinal ^1H relaxation rate (R_1; 30 MHz and 298 K) of diluted aqueous solutions of the two complexes were measured following the addition of increasing amount of HSA (PRE method, Fig. 4A). The analysis of the relaxometric binding isotherm allows estimating the affinity constant, K_A, for the protein and the relaxivity of the bound complex, r_1^b. Both Gd(III)-chelates interact with the protein, although to a different extent. The fit of the experimental data, performed considering two independent binding sites (n = 2), gave quite different values for the two complexes: K_A for Gd(AAZ3A-endoHB)-HSA is more than one order of magnitude higher than for Gd(AAZ3A-exoHB)-HSA (Table 4) probably due to the higher availability of the aromatic moiety to interact with the hydrophobic pocket of the protein. The stronger interaction of Gd(AAZ3A-endoHB) parallels to the longer distance and weaker interaction between Gd(III) and the phenolic oxygen with respect to Gd(AAZ3A-endoHB). Also r_1^b resulted to be three times greater for the Gd(AAZ3A-endoHB)-HSA adduct as a result of the two coordinated water molecules present in Gd(AAZ3A-endoHB).

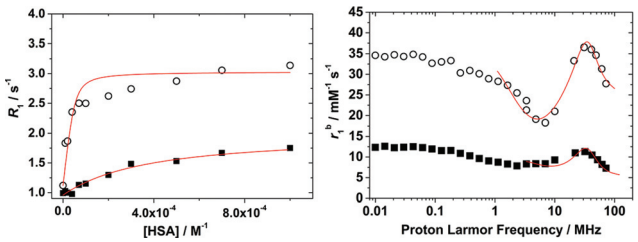

Fig. 4 (A) Water proton relaxation rate of aqueous solutions of Gd(AAZ3A-endoHB) (0.1 mM, circles) and Gd(AAZ3A-exoHB) (0.1 mM, squares) as a function of increasing amounts of HSA, measured at 20 MHz and 298 K. (B) $1/T_1$ NMRD profiles of the Gd(AAZ3A-endoHB)-HSA (circles) and Gd(AAZ3A-exoHB)-HSA adducts (squares), collected at 298 K. The solid lines through the data points are calculated using the parameters reported in Table 4. The data were analyzed only in the magnetic field region >1 T because of the known limitations of the SBM theory to completely account for the behaviour of slowly rotating systems at low magnetic field strengths.

The NMRD profiles of the two supramolecular adducts were recorded at neutral pH and 298 K under conditions ensuring that more than 98% of the chelate was bound to the protein (Fig. 4B). The high field region of the profiles (>1 T) was fitted to the SBM theory including the Lipari–Szabo approach for the description of the rotational dynamics.[38,39] This model considers a local rotation of the complex superimposed on the global reorientation of the supramolecular adduct. These two types of motion are characterized by different correlation times: τ_{RL} and τ_{RG}, respectively, related by the parameter S^2, which takes values between 0 (completely independent motions) and 1 (entirely correlated motions). A four-parameter (Δ^2, τ_V, τ_{RL} and S^2) least-squares fit of the data was performed and the best-fit parameters are listed in Table 4 and compared with the supramolecular system obtained by interacting an amphiphilic Gd(AAZTA)-like complex with HSA.[40] The analysis of the parameters remarks again the better interaction of Gd(AAZ3A-endoHB) with HSA than Gd(AAZ3A-exoHB), highlighted by the higher values of τ_{RL} and S^2, translated into a higher relaxivity (although caused also by the q = 2 of Gd(AAZ3A-endoHB)). Moreover, the comparison with the GdAAZTA-C_{12}-HSA adduct shows that the C_{12} alkyl chain strongly interacts with the hydrophobic pocket of HSA result-

Table 4 Selected best-fit parameters obtained from the analysis of the $1/T_1$ NMRD profiles of Gd(AAZ3A-endoHB)-HSA and Gd(AAZ3A-exoHB)-HSA adducts collected at 298 K compared to the analogous data obtained for Gd(AAZTA-C_{12})[40] [a]

Parameter	Gd(AAZ3A-endoHB)-HSA	Gd(AAZ3A-exoHB)-HSA	Gd(AAZTA C_{12})-HSA
$^{298}r_1$ (30 MHz) (mM^{-1} s^{-1})	36.5	11.4	52.5
$\Delta^2/10^{19}$ s^{-2}	2.4 ± 0.2	3.4 ± 0.2	1.5
$^{298}\tau_V$/ps	10 ± 2	42 ± 4	10
$^{298}\tau_M$/ns	160[b]	21.3	90
$^{298}\tau_{RG}$/ns	40	40	80
$^{298}\tau_{RL}$/ps	355 ± 20	98 ± 8	587
S^2	0.23 ± 0.01	0.07 ± 0.01	0.18
q	2	1	2
K_A/M^{-1}	7.5×10^4	1.5×10^3	8.5×10^4

[a] The distance of the hydrogen atoms of the coordinated water molecule from the metal ion (r_{GdH}) was fixed to 3.0 Å. The outer-sphere component of the relaxivity was estimated by using standard values for the distance of closest approach a (4 Å) and the relative diffusion coefficient of solute and solvent D (2.25×10^{-5} cm^2 s^{-1}). [b] The average between τ_M^A and τ_M^B for Gd(AAZ3A-endoHB) was used.

ing also into a slower local rotation of the complex around the alkyl chain (higher τ_{RL} value).

Conclusions

In conclusion we have highlighted the importance of ligand topology in two AAZ3A-HB chelators, which has a huge effect on the hydration number, stability and dissociation kinetics of two regioisomeric Gd(III) complexes. In fact, the replacement of an endocyclic acetate group of AAZTA with a 2-hydroxybenzyl group results in a q = 2 Gd-complex with higher relaxivity (5.9 mM^{-1} s^{-1} at 20 MHz and 310 K), but lower thermodynamic stability ($\log K_{GdL}$ = 19.57) and kinetic inertness ($t_{1/2}$ = 15.8 h at pH 7.4). Contrarily, the insertion of the phenolic pendant on the exocyclic nitrogen allows the formation of a more compact octadentate q = 1 Gd(III) complex with lower relaxivity (4.0 mM^{-1} s^{-1} at 20 MHz and 310 K), but remarkable stability ($\log K_{GdL}$ = 25.06) and good kinetic inertness ($t_{1/2}$ = 960 h at pH 7.4). The relevance of ligand topology has also nicely recently been demonstrated for a highly inert constrained pentaazamacrocyclic Cu(II) complex.[41] The different properties of metal complexes with regioisomeric ligands have been highlighted previously in other examples, *i.e.* the Mn(II) complexes of 1,4- and 1,7-DO2A which showed different hydration, and thus different relaxivities,[42] but similar thermodynamic stability and kinetic inertness.[43] However, the remarkable $\Delta \log K_{GdL}$ of 5.5 between AAZ3A-exo and endoHB Gd(III) complexes shows that in this case the ligand topology plays a remarkable role in metal ion coordination properties.

Experimental section

Chemicals and materials

All chemicals were purchased from commercial sources and were used without further purification unless otherwise stated. NMR spectra were recorded on Bruker Avance III spectrometers operating at 9.39 and 11.74 T, corresponding to protonic resonance frequencies of 399.8 and 499.8 MHz. ^{1}H and ^{13}C NMR chemical shifts are reported relative to TMS and are referenced using the residual proton solvent resonances. Splitting patterns are described as singlet (s), broad singlet (bs), doublet (d), triplet (t) or multiplet (m). ESI mass spectra were recorded on a Waters SQD 3100 (Waters Corporation, Milford, MA, USA). Analytical HPLC-MS were carried out on Waters modular system equipped with Waters 1525 binary pump, Waters 2487 UV/Vis and Waters SQD 3100 (ESCI ionization mode) detectors, using an XBridge™ Phenyl 3.5 µm 4.6 × 150 mm column (Waters). Semi-preparative HPLC purifications were performed with an XBridge™ Prep Phenyl 5 µm OBD™ 19 × 100 mm column (Waters). The HPLC methods are reported in the ESI.†

Synthesis

***N*,*N*,1-Tris(*tert*-butylacetate)-4-(2-acetoxybenzyl)-6-methyl-6-aminoperhydro-1,4-diazepine (2).** Compound **1** (0.14 g, 0.25 mmol) was dissolved in MeOH. 10 w/w% Pd/C (0.014 g) was added and the suspension was stirred under H_2-atmosphere (balloon) at room temperature overnight. After filtration through Celite and evaporation of the filtrate, the obtained debenzylated intermediate was dissolved in MeCN (10 mL). K_2CO_3 (0.066 g, 0.48 mmol) was added followed by 2-(bromomethyl)phenyl acetate (0.11 g, 0.48 mmol), and the suspension was refluxed overnight. After evaporation of the solvent, the residue was suspended in EtOAc (20 mL) and washed with H_2O (2 × 10 mL) and brine (10 mL). The organic phase was dried over anhydrous Na_2SO_4, filtered and evaporated. The crude product was purified by flash chromatography (SiO_2, PE/EtOAc 80 : 20, R_f = 0.20), leading to the aimed product as a yellow oil (0.048 g, 0.077 mmol, 32%).

^{1}H NMR (500 MHz, 25 °C, $CDCl_3$), δ (ppm): 7.55 (d, $^3J_{HH}$ = 7.0 Hz, 1H, CH^{Ar}), 7.21 (m, 2H, 2 × CH^{Ar}), 6.97 (d, $^3J_{HH}$ = 7.5 Hz, 1H, CH^{Ar}), 3.72 (s, 4H, $N(CH_2CO)_2$), 3.54 (d, $^2J_{HH}$ = 13.9 Hz, 1H, NCHH′Ar), 3.42 (d, $^2J_{HH}$ = 13.9 Hz, 1H, NCHH′Ar), 3.25 (s, 2H, NCH_2CO), 3.05 (d, $^2J_{HH}$ = 14.3 Hz, 1H, NCHH′CN), 2.99 (d, $^2J_{HH}$ = 13.6 Hz, 1H, NCH″H‴CN), 2.73 + 2.63 + 2.47 + 2.35 (m, 4H, NCH_2CH_2N), 2.67 (d, $^2J_{HH}$ = 14.3 Hz, 1H, NCHH′CN), 2.53 (d, $^2J_{HH}$ = 13.6 Hz, 1H, NCH″H‴CN), 2.30 (s, 3H, CH_3CO), 1.42 (s, 27H, $CH_3{}^{tBu}$), 1.04 (s, 3H, CH_3). ^{13}C NMR (125 MHz, 25 °C, $CDCl_3$), δ (ppm): 172.8 ($N(CH_2CO)_2$), 170.9 (NCH_2CO), 169.2 (CH_3CO), 149.1 (OC^{Ar}), 131.8 (CH_2C^{Ar}), 130.3 (CH^{Ar}), 127.7 (CH^{Ar}), 126.0 (CH^{Ar}), 122.1 (CH^{Ar}), 80.4 (C^{tBu}), 67.7 (NCH_2CN), 66.4 ($NC'H_2CN$), 62.1 (NCH_2CO), 60.7 ($NCCH_3$), 59.2 (NCH_2CH_2N), 58.1 (NCH_2Ar), 51.6 ($N(CH_2CO)_2$), 28.2 ($CH_3{}^{tBu}$), 24.2 ($NCCH_3$), 20.9 (CH_3CO). ESI$^+$ MS: m/z 620.6 [M + H^+], calc. for $[C_{33}H_{54}N_3O_8]^+$ = 620.80 g mol^{-1}.

AAZ3A-endoHB. Intermediate **2** (0.38 g, 0.61 mmol) was dissolved in THF (40 mL), 1 M NaOH (40 mL) was added and the biphasic system was stirred vigorously at 60 °C for 3 h. The solvents were evaporated and the residue was suspended in EtOAc (100 mL) and washed with H_2O (2 × 50 mL) and brine (50 mL). The organic phase was dried over anhydrous $MgSO_4$, filtered and evaporated. The obtained residue was dissolved in DCM (10 mL), triisopropylsilane (2 drops) and TFA (10 mL) were added and the solution was stirred at room temperature overnight. After removal of the volatiles under reduced pressure, the remaining solid was re-dissolved in TFA (1 mL) and precipitated in Et_2O (10 mL). The suspension was centrifuged (4000 rpm, 15 min, 10 °C) and the precipitate was washed/centrifuged with Et_2O (3 × 10 mL) and dried under vacuum. The product was purified by semi-preparative HPLC (see ESI†), re-dissolved in 1 M HCl (2 mL) and stirred for 2 h. The solution was evaporated, the residue dissolved in H_2O (2 mL) and lyophilized, and the product (mono hydrochloride salt) was obtained as a white powder (0.12 g, 0.26 mmol, 43%).

^{1}H NMR (500 MHz, 25 °C, D_2O), δ (ppm): 7.4–7.3 (m, 2H, 2 × CH^{Ar}), 6.94 (m, 2H, 2 × CH^{Ar}), 4.36 (d, $^2J_{HH}$ = 13.1 Hz, 2H, NCHH′Ar), 4.32 (d, $^2J_{HH}$ = 13.1 Hz, 2H, NCHH′Ar), 3.87 (m, 2H, $NCH_2CH'_2N$), 3.3–3.7 (m, 12H, 3 × NCH_2CO + 2 × NCH_2C + $NCH_2CH'_2N$), 1.12 (CH_3). ^{13}C NMR (125 MHz, 25 °C, D_2O), δ (ppm): 174.3 ($N(CH_2CO)_2$), 172.7 (NCH_2CO), 155.7 (COH^{Ar}), 133.1 + 132.3 + 120.9 + 116.1 (4 × CH^{Ar}), 115.6 (CH_2C^{Ar}), 62.8

(NCCH$_3$), 58.4 (3 × NCH$_2$CO), 57.3 (NCH$_2$Ar), 54.1 (NCH$_2$CH$_2$N), 51.7 (NCH$_2$CN), 49.7 (NCH′$_2$CN), 17.4 (CH$_3$). Elemental analysis: found C, 50.76; H, 6.45; N, 9.35; calc. for $C_{19}H_{28}ClN_3O_7$ C, 51.18; H, 6.33; N, 9.42. ESI$^+$ MS: *m*/*z* 410.4 [M + H$^+$], calc. for $[C_{19}H_{28}N_3O_7]^+$ = 410.44 g mol^{-1}.

***N*,1,4-Tris(*tert*-butylacetate)-*N*-(2-acetoxybenzyl)-6-methyl-6-aminoperhydro-1,4-diazepine (4).** Compound **3** (789 mg, 1.70 mmol) was dissolved in DMF (30 mL). K_2CO_3 (470 mg, 3.40 mmol) was added, followed by *tert*-butyl bromoacetate (0.30 mL, 2.04 mmol), and the mixture was stirred at 80 °C overnight. The solvent was evaporated under reduced pressure, the residue was suspended in EtOAc (40 mL) and washed with H_2O (2 × 20 mL) and brine (20 mL). The organic phase was dried over anhydrous Na_2SO_4, filtered and evaporated under vacuum. The crude product was purified by flash chromatography (SiO_2, DCM/MeOH 99 : 1 to 95 : 5, R_f (95 : 5) = 0.31), leading to the aimed compound as a yellow-colored oil (642 mg, 65%).

^{1}H NMR (500 MHz, 25 °C, $CDCl_3$), δ (ppm): 7.69 (m, 1H, CH^{Ar}), 7.17 (m, 1H, CH^{Ar}), 6.93 (m, 1H, CH^{Ar}), 4.03 (s, 2H, CH$_2$Ar), 3.38 (s, 2H, CH$_2$CO), 3.26 (s, 4H, 2 × CH$_2$CO), 3.13 (d, $^2J_{HH}$ = 13.9 Hz, 2H, NCHH′CN), 2.8–2.6 (m, 6H, NCHH′CN + NCH$_2$CH$_2$N), 1.42 + 1.33 (s, 27H, CH$_3$^{tBu}), 1.11 (s, 3H, CH$_3$). ^{13}C NMR (125 MHz, 25 °C, $CDCl_3$), δ (ppm): 172.8 + 170.9 (3 × COO*t*Bu), 148.8 (C^{Ar}), 133.2 (C^{Ar}), 130.1 (CH^{Ar}), 127.2 (CH^{Ar}), 126.2 (CH^{Ar}), 121.2 (CH^{Ar}), 80.7 + 80.0 (2 × C^{tBu}), 65.2 (NCH$_2$CN), 62.4 (2 × NCH$_2$CO), 59.1 (NCH$_2$CH$_2$N), 52.2 (NCH$_2$CO), 47.2 (CH$_2$Ar), 28.2 (CH$_3$^{tBu}), 20.8 (CH$_3$). ESI$^+$ MS: *m*/*z* 578.9 [M + H$^+$] (calc. for $[C_{31}H_{52}N_3O_7]^+$: 578.66 g mol^{-1}).

AAZ3A-exoHB. Intermediate **4** (0.24 mg, 0.41 mmol) was dissolved in DCM (2 mL), triisopropylsilane (3 drops) and TFA (2 mL) were added and the solution was stirred at room temperature for 5 h. After removal of the volatiles under reduced pressure, the residue was dissolved again in TFA (1 mL) and precipitated in Et$_2$O (10 mL). The suspension was centrifuged (4000 rpm, 15 min, 10 °C) and the precipitate was washed/centrifuged with Et$_2$O (3 × 10 mL) and dried under vacuum. The product was obtained as a white powder (57 mg, 65%).

^{1}H NMR (500 MHz, 25 °C, D_2O), δ (ppm): 7.4–7.3 (m, 2H, 2 × CH^{Ar}), 6.96 (m, 2H, 2 × CH^{Ar}), 4.38 (d, $^2J_{HH}$ = 13.1 Hz, 1H, CHH′Ar), 4.34 (d, $^2J_{HH}$ = 13.1 Hz, 1H, CHH′Ar), 3.6–3.4 (m, 10H, 3 × CH$_2$CO + 2 × NCH$_2$CN), 3.4–3.3 (m, 4H, NCH$_2$CH$_2$N), 1.11 (s, 3H, CH$_3$). ^{13}C NMR (125 MHz, 25 °C, D_2O), δ (ppm): 174.7 + 172.7 (3 × COOH), 155.7 (C^{Ar}), 133.1 (CH^{Ar}), 132.4 (CH^{Ar}), 120.9 (CH^{Ar}), 116.1 (CH^{Ar}), 115.6 (C^{Ar}), 62.3 (NCH$_2$CN), 58.9 + 58.3 + 58.1 (3 × NCH$_2$CO), 57.3 (CH$_2$Ar), 53.5 (NCH$_2$CN), 49.8 (NCH$_2$CH$_2$N), 17.7 (CH$_3$). Elemental analysis: found C, 54.96; H, 6.77; N, 10.09; calc. for $C_{19}H_{27}N_3O_7$ C, 55.74; H, 6.65; N, 10.26. ESI$^+$ MS: *m*/*z* 410.6 [M + H$^+$] (calc. for $[C_{19}H_{28}N_3O_7]^+$: 410.45 g mol^{-1}).

Thermodynamic studies

The chemicals used for the experiments were of the highest analytical grade. The concentration of the $GdCl_3$ and $EuCl_3$ solutions was determined by complexometric titration with standardized Na_2H_2EDTA and xylenol orange as indicators. The concentration of the H_4AAZ3A-endoHB and H_4AAZ3A-exoHB was determined by pH-potentiometric titration in the presence and absence of a large (40-fold) excess of $CaCl_2$. The pH-potentiometric titrations were made with standardized 0.2 M NaOH.

The stability and protonation constants of the Gd(III)-complexes of AAZ3A-endoHB and AAZ3A-exoHB ligands were determined by pH-potentiometric titration. The metal-to-ligand concentration ratio was 1 : 1 (the concentration of the ligand was generally 0.002 M). For the pH measurements and titrations, a Metrohm 888 Titrando automatic titration workstation with a Metrohm-6.0234.110 combined electrode was used. Equilibrium measurements were carried out at a constant ionic strength (0.15 M NaCl) in 6 mL samples at 25 °C under magnetic stirring and N_2 bubbling. The titrations were made in the pH range 1.7–12.0. KH-phthalate (pH = 4.005) and borax (pH = 9.177) buffers were used to calibrate the pH meter. For the calculation of [H$^+$] from the measured pH values, the method proposed by Irving *et al.* was used.[44] A 0.01 M HCl solution was titrated with the standardized NaOH solution in the presence of 0.15 M NaCl ionic strength. The differences (*A*) between the measured (pH_{read}) and calculated pH (−log[H$^+$]) values were used to obtain the equilibrium H$^+$ concentration from the pH values measured in the titration experiments (*A* = 0.035). The waiting time between two pH measurements was 60 s. For the equilibrium calculations, the stoichiometric water ionic product (pK_w) was also needed to calculate [OH$^-$] values under basic conditions. The V_{NaOH}–pH_{read} data pairs of the HCl–NaOH titration obtained in the pH range 10.5–12.0 were used to calculate the pK_w value (pK_w = 13.75).

The protonation constants of the phenolate group of both ligands and those of Gd(III)-complexes were also determined by spectrophotometry at the absorption band of the aromatic group. The absorption spectra of 0.1 mM solutions of AAZ3A-endoHB, Gd(AAZ3A-endoHB) and Gd(AAZ3A-exoHB) were recorded in the pH range 2–12 and in the wavelength range of 210–350 nm in 0.15 M NaCl. The pH was adjusted by stepwise addition of concentrated NaOH or HCl. The spectrophotometric measurements were made with the use of PerkinElmer Lambda 365 UV-Vis spectrophotometer at 25 °C, using 1.0 cm cells. The protonation and stability constants were calculated with the PSEQUAD program.[45]

Transmetallation reactions with Cu(II)

The kinetic inertness of Gd(AAZ3A-endoHB) and Gd(AAZ3A-exoHB) was determined by the rates of the Cu(II) mediated metal exchange reactions at different pH values. The exchange reactions with Cu(II) were studied by spectrophotometry, following the formation of the CuL complexes at 275 nm with PerkinElmer Lambda 365 UV-Vis spectrophotometer. The concentration of the Gd(AAZ3A-endoHB) complex was 0.2 mM, while the concentration of Cu(II) was 10 to 40 times higher, in order to guarantee pseudo-first-order conditions. The temperature was maintained at 25 °C and the ionic strength of the solutions was kept constant using 0.15 M NaCl. The exchange rates were studied in the pH range about 3.0–5.0. For keeping

the pH values constant, 1,4-dimethylpiperazine (pH range 3.0–4.1) and *N*-methylpiperazine (pH range 4.1–5.2) buffers (0.01 M) were used. The pseudo-first-order rate constants (k_d) were calculated by fitting the absorbance data to eqn (5)

$$A_t = (A_0 - A_p)e^{-k_d t} + A_p \quad (5)$$

where A_t, A_0 and A_p are the absorbance values at time t, the start of the reaction and at equilibrium, respectively. The calculation of the kinetic parameters were performed by the fitting of the absorbance–time and relaxation rate–time data pairs with the Micromath Scientist computer program (version 2.0, Salt Lake City, UT, USA).

Relaxometric measurements

The Gd(III) complexes were prepared by mixing solutions of $GdCl_3$ hexahydrate and the ligand (in *ca*. 5% molar excess) and adjusting the pH to about 6.5 with aqueous NaOH. The exact concentration of the aqueous solutions for ^{1}H NMRD and ^{17}O NMR measurements was determined by measuring the bulk magnetic susceptibility shifts of the *tert*-BuOH ^{1}H NMR signal at 11.7 T.[46] Proton relaxation measurements ($1/T_1$) and the resulting $1/T_1$ NMRD profiles were measured on a Fast-Field Cycling (FFC) Stelar SmarTracer Relaxometer (Stelar s.r.l., Mede (PV), Italy) over a continuum of magnetic field strengths from 0.00024 to 0.25 T (corresponding to 0.01–10 MHz proton Larmor frequencies). The relaxometer operates under computer control with an absolute uncertainty in $1/T_1$ of ±1%. A precise control of the temperature was operated during the measurements by means of a Stelar VTC-91 airflow heater equipped with a calibrated copper constantan thermocouple (uncertainty of ±0.1 °C). Furthermore, the real temperature inside the probe head was additionally monitored by a Fluke 52 k/j digital thermometer (Fluke, Zürich, Switzerland). Additional data in the 20–120 MHz frequency range were obtained with a High Field Relaxometer (Stelar) equipped with the HTS-110 3T Metrology Cryogen-free Superconducting Magnet. The data were collected using the standard inversion recovery sequence (20 experiments, 2 scans) with a typical 90° pulse width of 3.5 ms and the reproducibility of the data was within ±0.5%. ^{17}O NMR spectra were recorded on a Bruker Avance III spectrometer (11.7 T) equipped with a 5 mm probe and a standard temperature control unit. Aqueous solutions of the complexes (*ca*. 6–10 mM) containing 2.0% of the ^{17}O isotope (Cambridge Isotope Laboratories Inc., Tewksbury, MA, USA) were used. The observed transverse relaxation rates were calculated from the signal width at half-height as a function of temperature in the 278–350 K range.

Theoretical calculations

Optimizations of the $[Gd(L)(H_2O)_2]^-\cdot 4H_2O$ systems (L = AAZ3A-endoHB or AAZ3A-exoHB) were performed with the Gaussian 16 program package (revision B.01), using the pseudopotential approximation and the wB97XD functional,[27] which includes empirical dispersion. We selected the quasirelativistic large-core pseudopotential of the Stuttgart/Cologne group (46 + 4f7 electrons in the core for Gd) and the related [5s4p3d] valence basis set,[28] while the standard 6-311G(d,p) basis set was used for all other atoms. No restraints were imposed for geometry optimization and frequency calculations were used to confirm the nature of the optimized geometries as local energy minima. The output of frequency calculations provided the thermal contributions and zero-point energies required to calculate the enthalpy and entropy of the systems. Bulk solvent effects (water) were considered with integral equation formalism of the polarized continuum model (IEFPCM), using the default parameters implemented in Gaussian 16.[47] The size of the integration grid was increased with the integral = ultrafine keyword.

Scalar relativistic calculations were performed with the ORCA program package[34] using the second-order Douglas–Kroll–Hess method.[36,48] Solvent effects (water) were included with the SMD solvation model.[49] DFT calculations used the TPSSh functional,[35] in combination with the SARC2-DKH-QZVP[37] basis set for Gd and the DKH-def2-TZVPP[50,51] basis set for all other atoms. The resolution of identity and chain of spheres RIJCOSX approximation[52] was used to speed up the calculations using the Autoaux[53] procedure to generate auxiliary basis sets for Gd and the SARC/J basis set for other atoms. The quasi-restricted orbitals generated from these calculations were used as starting orbitals for CASSCF/NEVPT2[54,55] calculations, in which the active space included 7 electrons distributed in the seven 4f-based orbitals (1 octet root and 49 sextets were considered). The RIJCOSX approximation[56] was used also in these calculations, with the SARC2-DKH-QZVP/JK[37] auxiliary basis set for Gd and the Autoaux[53] procedure to generate auxiliary basis sets for all other atoms. Spin–orbit coupling effects were included by using quasi-degenerate perturbation theory (QDPT).[57] All ORCA calculations used a Gaussian finite nucleus model.[58]

Conflicts of interest

There are no conflicts to declare.

References

1 S. Aime, L. Calabi, C. Cavallotti, E. Gianolio, G. B. Giovenzana, P. Losi, A. Maiocchi, G. Palmisano and M. Sisti, [GdAAZTA]$^-$: A new structural entry for an improved generation of MRI contrast agents, *Inorg. Chem.*, 2004, **43**, 7588–7590.

2 J. P. Sinnes, U. Bauder-Wüst, M. Schäfer, E. S. Moon, K. Kopka and F. Rösch, ^{68}Ga, ^{44}Sc and ^{177}Lu-labeled AAZTA5-PSMA-617: synthesis, radiolabeling, stability and cell binding compared to DOTA-PSMA-617 analogues, *EJNMMI Radiopharm. Chem.*, 2020, **5**, 28.

3 J.-P. Sinnes, J. Nagel, B. P. Waldron, T. Maina, B. A. Nock, R. K. Bergmann, M. Ullrich, J. Pietzsch, M. Bachmann, R. P. Baum and F. Rösch, Instant kit preparation of ^{68}Ga-

radiopharmaceuticals via the hybrid chelator DATA: clinical translation of [^{68}Ga]Ga-DATA-TOC, *EJNMMI Res.*, 2019, **9**, 48.

4 G. Nagy, D. Szikra, G. Trencsenyi, A. Fekete, I. Garai, A. M. Giani, R. Negri, N. Masciocchi, A. Maiocchi, F. Uggeri, I. Toth, S. Aime, G. B. Giovenzana and Z. Baranyai, AAZTA: An Ideal Chelating Agent for the Development of Sc-44 PET Imaging Agents, *Angew. Chem., Int. Ed.*, 2017, **56**, 2118–2122.

5 S. Ghiani, I. Hawala, D. Szikra, G. Trencsényi, Z. Baranyai, G. Nagy, A. Vágner, R. Stefania, S. Pandey and A. Maiocchi, Synthesis, radiolabeling, and pre-clinical evaluation of [^{44}Sc]Sc-AAZTA conjugate PSMA inhibitor, a new tracer for high-efficiency imaging of prostate cancer, *Eur. J. Nucl. Med. Mol. Imaging*, 2021, **48**, 2351–2362.

6 Z. Baranyai, F. Uggeri, A. Maiocchi, G. B. Giovenzana, C. Cavallotti, A. Takacs, I. Toth, I. Banyai, A. Benyei, E. Brucher and S. Aime, Equilibrium, Kinetic and Structural Studies of AAZTA Complexes with Ga^{3+}, In^{3+} and Cu^{2+}, *Eur. J. Inorg. Chem.*, 2013, 147–162.

7 D. D. Castelli, L. Tei, F. Carniato, S. Aime and M. Botta, [Yb(AAZTA)(H_2O)]$^-$: an unconventional ParaCEST MRI probe, *Chem. Commun.*, 2018, **54**, 2004–2007.

8 Z. Baranyai, D. Delli Castelli, C. Platas-Iglesias, D. Esteban-Gomez, A. Bényei, L. Tei and M. Botta, Combined NMR, DFT and X-ray studies highlight structural and hydration changes of [Ln(AAZTA)]$^-$ complexes across the series, *Inorg. Chem. Front.*, 2020, **7**, 795–803.

9 D. Lalli, F. Carniato, L. Tei, C. Platas-Iglesias and M. Botta, Surprising complexity of the [Gd(AAZTA)(H_2O)$_2$]$^-$ chelate revealed by NMR in the frequency and time domains, *Inorg. Chem.*, 2022, **61**, 496–506.

10 C. Robic, M. Port, O. Rousseaux, S. Louguet, N. Fretellier, S. Catoen, C. Factor, S. Le Greneur, C. Medina, P. Bourrinet, I. Raynal, J.-M. Idée and C. Corot, Physicochemical and pharmacokinetic profiles of Gadopiclenol: a new macrocyclic gadolinium chelate with high T_1 relaxivity, *Invest. Radiol.*, 2019, **54**, 475–484.

11 A. Vagner, C. D'Alessandria, G. Gambino, M. Schwaiger, S. Aime, A. Maiocchi, I. Toth, Z. Baranyai and L. Tei, A rigidified AAZTA-like ligand as efficient chelator for Ga-68 radiopharmaceuticals, *ChemistrySelect*, 2016, **1**, 163–171.

12 A. Vagner, E. Gianolio, S. Aime, A. Maiocchi, I. Toth, Z. Baranyai and L. Tei, High kinetic inertness of a bis-hydrated Gd-complex with a constrained AAZTA-like ligand, *Chem. Commun.*, 2016, **52**, 11235–11238.

13 L. Tei, G. Gugliotta, D. Marchi, M. Cossi, S. Geninatti Crich and M. Botta, Optimizing the relaxivity at high fields: systematic variation of the rotational dynamics in polynuclear Gd-complexes based on the AAZTA ligand, *Inorg. Chem. Front.*, 2021, **8**, 4806–4819.

14 D. L. Longo, F. Arena, L. Consolino, P. Minazzi, S. Geninatti-Crich, G. B. Giovenzana and S. Aime, Gd-AAZTA-MADEC, an improved blood pool agent for DCE-MRI studies on mice on 1 T scanners, *Biomaterials*, 2016, **75**, 47–57.

15 F. Carniato, L. Tei, J. Martinelli and M. Botta, Relaxivity Enhancement of Ditopic Bishydrated Gadolinium(III) Complexes Conjugated to Mesoporous Silica Nanoparticles, *Eur. J. Inorg. Chem.*, 2018, 2363–2368.

16 A. Ermelindo, G. Gambino and L. Tei, Synthesis of a mixed carboxylate-phosphinate AAZTA-like ligand and relaxometric characterization of its Gd(III) complex, *Tetrahedron Lett.*, 2013, **54**, 6378–6380.

17 C. Guanci, R. Pinalli, S. Aime, E. Gianolio, L. Lattuada and G. B. Giovenzana, Synthesis of phosphonic analogues of AAZTA and relaxometric evaluation of the corresponding Gd(III) complexes as potential MRI contrast agents, *Tetrahedron Lett.*, 2015, **56**, 1994–1997.

18 C. V. Esteves, J. Madureira, L. M. P. Lima, P. Mateus, I. Bento and R. Delgado, Copper(II) and Gallium(III) Complexes of trans-bis(2-hydroxybenzyl) cyclen derivatives: absence of a cross-bridge proves surprisingly more favorable, *Inorg. Chem.*, 2014, **53**, 4371–4386.

19 J. Martinelli, D. Remotti and L. Tei, Selective functionalization of 6-amino-6-methyl-1,4-perhydrodiazepine for the synthesis of a library of polydentate chelators, *Org. Biomol. Chem.*, 2020, **18**, 5245–5252.

20 E. Kimura, T. Koike, K. Uenishi, M. Hediger, M. Kuramoto, S. Joko, Y. Arai, M. Kodama and Y. Iitaka, New-dimensional cyclam. Synthesis, crystal structure, and chemical properties of macrocyclic tetraamines bearing a phenol pendant, *Inorg. Chem.*, 1987, **26**, 2975–2983.

21 E. Farkas, J. Nagel, B. P. Waldron, D. Parker, I. Toth, E. Brucher, F. Rosch and Z. Baranyai, Equilibrium, Kinetic and Structural Properties of Gallium(III) and Some Divalent Metal Complexes Formed with the New DATA(m) and DATA(5 m) Ligands, *Chem. – Eur. J.*, 2017, **23**, 10358–10371.

22 E. Farkas, A. Vagner, R. Negri, L. Lattuada, I. Toth, V. Colombo, D. Esteban-Gomez, C. Platas-Iglesias, J. Notni, Z. Baranyai and G. B. Giovenzana, PIDAZTA: Structurally Constrained Chelators for the Efficient Formation of Stable Gallium-68 Complexes at Physiological pH, *Chem. – Eur. J.*, 2019, **25**, 10698–10709.

23 Z. Baranyai, F. Uggeri, G. B. Giovenzana, A. Benyei, E. Bruecher and S. Aime, Equilibrium and Kinetic Properties of the Lanthanoids(III) and Various Divalent Metal Complexes of the Heptadentate Ligand AAZTA, *Chem. – Eur. J.*, 2009, **15**, 1696–1705.

24 S. Hajela, M. Botta, S. Giraudo, J. Xu, K. N. Raymond and S. Aime, A Tris-hydroxymethyl-Substituted Derivative of Gd-TREN-Me-3,2-HOPO: An MRI Relaxation Agent with Improved Efficiency, *J. Am. Chem. Soc.*, 2000, **122**, 11228–11229.

25 Z. Baranyai, Z. Palinkas, F. Uggeri and E. Brucher, Studies on the Gd^{3+}, Cu^{2+} and Zn^{2+} Complexes of BOPTA, DTPA and DTPA-BMA Ligands: Kinetics of Metal-Exchange Reactions of [Gd(BOPTA)]$^{2-}$, *Eur. J. Inorg. Chem.*, 2010, 1948–1956.

26 W. P. Cacheris, S. K. Nickle and A. D. Sherry, Thermodynamic Study of Lanthanide Complexes of 1,4,7-

Triazacyclononane-N,N′,N″-Triacetic Acid and 1,4,7,10-Tetraazacyclododecane-N,N′,N″,N‴-Tetraacetic Acid, *Inorg. Chem.*, 1987, **26**, 958–960.

27 J. D. Chai and M. Head-Gordon, Long-range corrected hybrid density functionals with damped atom-atom dispersion corrections, *Phys. Chem. Chem. Phys.*, 2008, **10**, 6615–6620.

28 M. Dolg, H. Stoll, A. Savin and H. Preuss, Energy-adjusted pseudopotentials for the rare earth elements, *Theor. Chim. Acta*, 1989, **75**, 173–194.

29 D. Esteban-Gomez, A. de Blas, T. Rodriguez-Blas, L. Helm and C. Platas-Iglesias, Hyperfine Coupling Constants on Inner-Sphere Water Molecules of Gd(III)-Based MRI Contrast Agents, *ChemPhysChem*, 2012, **13**, 3640–3650.

30 L. Leone, D. Esteban-Gomez, C. Platas-Iglesias, M. Milanesio and L. Tei, Accelerating water exchange in Gd(III)-DO3A-derivatives by favouring the dissociative mechanism through hydrogen bonding, *Chem. Commun.*, 2019, **55**, 513–516.

31 S. Aime, M. Botta, D. Esteban-Gómez and C. Platas-Iglesias, Characterisation of magnetic resonance imaging (MRI) contrast agents using NMR relaxometry, *Mol. Phys.*, 2019, **117**, 898–909.

32 L. Tei, G. Gugliotta, Z. Baranyai and M. Botta, A new bifunctional Gd(III) complex of enhanced efficacy for MR-molecular imaging applications, *Dalton Trans.*, 2009, 9712–9714.

33 R. Ruloff, E. Toth, R. Scopelliti, R. Tripier, H. Handel and A. E. Merbach, Accelerating water exchange for Gd(III) chelates by steric compression around the water binding site, *Chem. Commun.*, 2002, 2630–2631.

34 F. Neese, Software update: the ORCA program system, version 4.0, *Wiley Interdiscip. Rev.: Comput. Mol. Sci.*, 2018, **8**, e1327.

35 J. M. Tao, J. P. Perdew, V. N. Staroverov and G. E. Scuseria, Climbing the density functional ladder: Nonempirical meta-generalized gradient approximation designed for molecules and solids, *Phys. Rev. Lett.*, 2003, **91**, 146401.

36 M. Reiher, Douglas-Kroll-Hess Theory: a relativistic electrons-only theory for chemistry, *Theor. Chem. Acc.*, 2006, **116**, 241–252.

37 D. Aravena, F. Neese and D. A. Pantazis, Improved Segmented All-Electron Relativistically Contracted Basis Sets for the Lanthanides, *J. Chem. Theory Comput.*, 2016, **12**, 1148–1156.

38 G. Lipari and A. Szabo, Model-free approach to the interpretation of nuclear magnetic resonance relaxation in macromolecules. 1. Theory and range of validity, *J. Am. Chem. Soc.*, 1982, **104**, 4546–4559.

39 G. Lipari and A. Szabo, Model-free approach to the interpretation of nuclear magnetic resonance relaxation in macromolecules. 2. Analysis of experimental results, *J. Am. Chem. Soc.*, 1982, **104**, 4559–4570.

40 G. Gambino, L. Tei, F. Carniato and M. Botta, Amphiphilic Ditopic Bis-Aqua Gd-AAZTA-like Complexes Enhance Relaxivity of Lipidic MRI Nanoprobes, *Chem. – Asian J.*, 2016, **11**, 2139–2143.

41 A. D. Shircliff, B. P. Burke, D. J. Davilla, G. E. Burgess, F. A. Okorocha, A. Shrestha, E. M. A. Allbritton, P. T. Nguyen, R. L. Lamar, D. G. Jones, M. J. Gorbet, M. B. Allen, J. I. Eze, A. T. Fernandez, D. Ramirez, S. J. Archibald, T. J. Prior, J. A. Krause, A. G. Oliver and T. J. Hubin, An ethylene cross-bridged pentaazamacrocycle and its Cu^{2+} complex: constrained ligand topology and excellent kinetic stability, *Chem. Commun.*, 2020, **56**, 7519–7522.

42 G. A. Rolla, C. Platas-Iglesias, M. Botta, L. Tei and L. Helm, ^{1}H and ^{17}O NMR Relaxometric and Computational Study on Macrocyclic Mn(II) Complexes, *Inorg. Chem.*, 2013, **52**, 3268–3279.

43 Z. Garda, A. Forgács, Q. N. Do, F. K. Kálmán, S. Timári, Z. Baranyai, L. Tei, I. Tóth, Z. Kovács and G. Tircsó, Physico-chemical properties of Mn(II) complexes formed with cis- and trans-DO2A: thermodynamic, electrochemical and kinetic studies, *J. Inorg. Biochem.*, 2016, **163**, 206–213.

44 H. M. Irving, M. G. Miles and L. D. Pettit, A study of some problems in determining the stoicheiometric proton dissociation constants of complexes by potentiometric titrations using a glass electrode, *Anal. Chim. Acta*, 1967, **38**, 475–488.

45 L. Zékány and I. Nagypál, *Computational Method for Determination of Formation Constants*, ed. D. J. Legett, Plenum Press, New York, 1985, p. 291.

46 D. M. Corsi, C. Platas-Iglesias, H. van Bekkum and J. A. Peters, Determination of paramagnetic lanthanide(III) concentrations from bulk magnetic susceptibility shifts in NMR spectra, *Magn. Reson. Chem.*, 2001, **39**, 723–726.

47 J. Tomasi, B. Mennucci and R. Cammi, Quantum mechanical continuum solvation models, *Chem. Rev.*, 2005, **105**, 2999–3093.

48 M. Barysz and A. J. Sadlej, Two-component methods of relativistic quantum chemistry: from the Douglas-Kroll approximation to the exact two-component formalism, *J. Mol. Struct.: THEOCHEM*, 2001, **573**, 181–200.

49 A. V. Marenich, C. J. Cramer and D. G. Truhlar, Universal Solvation Model Based on Solute Electron Density and on a Continuum Model of the Solvent Defined by the Bulk Dielectric Constant and Atomic Surface Tensions, *J. Phys. Chem. B*, 2009, **113**, 6378–6396.

50 D. A. Pantazis, X. Y. Chen, C. R. Landis and F. Neese, All-electron scalar relativistic basis sets for third-row transition metal atoms, *J. Chem. Theory Comput.*, 2008, **4**, 908–919.

51 F. Weigend and R. Ahlrichs, Balanced basis sets of split valence, triple zeta valence and quadruple zeta valence quality for H to Rn: Design and assessment of accuracy, *Phys. Chem. Chem. Phys.*, 2005, **7**, 3297–3305.

52 F. Neese, F. Wennmohs, A. Hansen and U. Becker, Efficient, approximate and parallel Hartree-Fock and hybrid DFT calculations. A "chain-of-spheres" algorithm for the Hartree-Fock exchange, *Chem. Phys.*, 2009, **356**, 98–109.

53 G. L. Stoychev, A. A. Auer and F. Neese, Automatic Generation of Auxiliary Basis Sets, *J. Chem. Theory Comput.*, 2017, **13**, 554–562.

54 C. Angeli, S. Borini, M. Cestari and R. Cimiraglia, A quasi-degenerate formulation of the second order n-electron valence state perturbation theory approach, *J. Chem. Phys.*, 2004, **121**, 4043–4049.
55 C. Angeli, R. Cimiraglia, S. Evangelisti, T. Leininger and J. P. Malrieu, Introduction of n-electron valence states for multireference perturbation theory, *J. Chem. Phys.*, 2001, **114**, 10252–10264.
56 C. Kollmar, K. Sivalingam, B. Helmich-Paris, C. Angeli and F. Neese, A perturbation-based super-CI approach for the orbital optimization of a CASSCF wave function, *J. Comput. Chem.*, 2019, **40**, 1463–1470.
57 L. Lang and F. Neese, Spin-dependent properties in the framework of the dynamic correlation dressed complete active space method, *J. Chem. Phys.*, 2019, **150**, 104104.
58 L. Visscher and K. G. Dyall, Dirac-Fock atomic electronic structure calculations using different nuclear charge distributions, *At. Data Nucl. Data Tables*, 1997, **67**, 207–224.
59 E. M. Elemento, D. Parker, S. Aime, E. Gianolio and L. Lattuada, Variation of water exchange dynamics with ligand structure and stereochemistry in lanthanide complexes based on 1,4-diazepine derivatives, *Org. Biomol. Chem.*, 2009, **7**, 1120–1131.